euronoise 2021
25th to 27th of October
Madeira, Portugal - online

Hybrid Fourier pseudospectral/discontinuous Galerkin time-domain method for urban sound propagation in a moving atmosphere

Matthias Cosnefroy*, **Maarten Hornikx**

Department of the Built Environment, Eindhoven University of Technology, Eindhoven, The Netherlands

*{m.h.r.cosnefroy@tue.nl}

Abstract

The Fourier Pseudospectral time-domain (Fourier PSTD) method and the nodal Discontinuous Galerkin (DG) method are both able to effectively solve the Linearized Euler Equations (LEE). The two approaches however suffer from limitations in the context of outdoor sound propagation, as Fourier PSTD has difficulties modeling complex boundaries (buildings, topography, frequency-dependent boundary properties) while the computational cost associated with DG can quickly become prohibitive for large-scale simulations. Previous studies have shown that the two methods can be coupled with the use of a buffer zone enabling data exchange between the solvers, to take advantage of the geometrical flexibility of DG close to the boundaries and of the cost-efficiency of Fourier PSTD in the bulk of the domain. The current work extends the hybrid methodology to take into account the full wind velocity vector, as opposed to the effective sound speed approximation.

Keywords: Outdoor sound propagation, linearized Euler equations, discontinuous Galerkin, Fourier pseudospectral, hybrid time-domain method

1 Introduction

Accurate prediction of outdoor acoustics still proves challenging due to the combined influence of the ground surface and micrometeorology on sound propagation, especially at long range. These effects are usually frequency-dependent and can include absorption, reflection and diffraction from the ground and from obstacles (such as buildings), refraction due to wind and temperature gradients, or scattering by turbulence. Numerous numerical methods were developed to try and account for these phenomena. Over the last decades, wave-based methods, in particular, have gained significant traction due to the rapid growth in computing power and due to their ability to directly solve the linearized Euler equations (LEE) in the time domain, with few inherent assumptions; these methods are however still limited in application.

To name only a few, the finite-difference time-domain (FDTD) and the Fourier pseudospectral (PSTD) methods are well-established and popular choices among the outdoor sound propagation community [1, 2, 3, 4], due to their computational efficiency and relative ease of implementation. Both methods, however, have difficulties modeling arbitrary boundary shapes, and, for PSTD, modeling frequency-dependent boundary properties [5]. At the other hand of the spectrum, the nodal discontinuous Galerkin (DG) method [6, 7, 8] only recently gained interest for outdoor acoustics, and features almost no restriction regarding the modeling of complex geometries and boundary conditions; this geometrical flexibility comes at the cost of more stringent requirements on the spatial and temporal discretization, which can render the computational cost prohibitive for large-scale simulations.

A recent study [9] proposed a hybrid methodology where the DG method is used in the vicinity of boundaries while the PSTD method is used in the bulk of the domain, in order to retain the benefits of both approaches. The procedure hinges on a conformal coupling zone between the overlapping DG and PSTD domains, allowing for data exchange between the solvers. The proposed hybrid solver could be readily used for outdoor acoustics by incorporating the wind effects via the effective sound speed approach [10]; this approximation is however

known to be valid only for small elevation angles from the source, which could limit the applicability of the model. The current work aims at implementing the effects of a moving inhomogeneous atmosphere into the hybrid model by explicitly solving the LEE in the presence of wind.

The paper is organized as follows. Section 2 presents the new DG formulation used to solve the LEE. Section 3 briefly presents the PSTD solver and recalls the hybrid PSTD-DG methodology. The accuracy of the new hybrid solver in then assessed in the presence of wind, in Section 4, with two benchmark cases.

2 The nodal discontinuous Galerkin method for outdoor sound propagation

2.1. Linearized Euler equations

Linearized Euler equations (LEE) describing the propagation of sound waves in a moving inhomogeneous atmosphere can be obtained from the laws of conservation of mass, momentum and energy. If the acoustic fluctuations are small compared to the atmospheric parameters, and if air can be considered as an ideal gas, the following coupled equations can be obtained [11]:

$$\frac{\partial p}{\partial t} + \mathbf{u} \cdot \nabla p + \rho_0 c^2 \, \nabla \cdot \mathbf{v} = \rho_0 c^2 \, Q \,, \tag{1}$$

$$\frac{\partial \mathbf{v}}{\partial t} + (\mathbf{u} \cdot \nabla) \, \mathbf{v} + (\mathbf{v} \cdot \nabla) \, \mathbf{u} + \nabla p / \rho_0 = \mathbf{F} / \rho_0 \,, \tag{2}$$

with p the acoustic pressure and $\mathbf{v} = (v_x, v_y)$ the particle velocity vector, at time t and location $\mathbf{r} = (x, y)$; a 2D propagation is considered in this work to reduce the computational costs, although the model can be generalized to 3D. The propagation medium is defined by the air density ρ_0, the adiabatic sound speed c and the wind vector $\mathbf{u} = (u_x, u_y)$; these parameters are assumed known and are constant over time, but can vary spatially. The variables Q and $\mathbf{F} = (F_x, F_y)$ account for potential mass sources and external forces, respectively. The terms of order higher than or equal to $|\mathbf{v}|^2 / c^2$ were neglected to obtain this set of equations, and the wave equation can be recovered for $\mathbf{u} = \mathbf{0}$. For numerical purposes, and assuming a two-dimensional propagation, Eqs. (1) and (2) can be cast into the following matrix form:

$$\frac{\partial \mathbf{q}}{\partial t} + \mathbf{A}_x \frac{\partial \mathbf{q}}{\partial x} + \mathbf{A}_y \frac{\partial \mathbf{q}}{\partial y} + \mathbf{B}\mathbf{q} = \mathbf{S} \,, \tag{3}$$

with $\mathbf{q} = \{p, v_x, v_y\}^T$ the solution vector, and

$$\mathbf{A}_i = \begin{bmatrix} u_i & \rho_0 c^2 \delta_{ix} & \rho_0 c^2 \delta_{iy} \\ \delta_{ix}/\rho_0 & u_i & 0 \\ \delta_{iy}/\rho_0 & 0 & u_i \end{bmatrix}, \quad \mathbf{B} = \begin{bmatrix} 0 & 0 & 0 \\ 0 & \dfrac{\partial u_x}{\partial x} & \dfrac{\partial u_x}{\partial y} \\ 0 & \dfrac{\partial u_y}{\partial x} & \dfrac{\partial u_y}{\partial y} \end{bmatrix}, \quad \mathbf{S} = \begin{Bmatrix} \rho_0 c^2 Q \\ F_x/\rho_0 \\ F_y/\rho_0 \end{Bmatrix},$$

with $i = \{x, y\}$ and the Kronecker delta function δ_{ij} to simplify the notations. The diagonal entries of $\mathbf{A}_i$ and the matrix $\mathbf{B}$ are responsible for the effects of the wind.

System (3) is to be solved numerically with the DG method from the (known) initial solution vector $\mathbf{q}(\mathbf{r}, t = 0)$ and together with appropriate boundary conditions.

2.2. Numerical formulation

To derive the DG methodology, the physical domain Ω is first partitioned into a set of non-overlapping and unstructured elements Ω_e. The variational formulation of the LEE is then obtained as a projection of the piecewise test functions $\mathbf{\Phi}_e$ over Ω_e, and two consecutive integrations by parts allow to derive the corresponding

strong formulation[1]:

$$\int_{\Omega_e} \mathbf{\Phi}_e^T \left[\frac{\partial \mathbf{q}_e}{\partial t} + \mathbf{A}_x \frac{\partial \mathbf{q}_e}{\partial x} + \mathbf{A}_y \frac{\partial \mathbf{q}_e}{\partial y} + \mathbf{B}\mathbf{q}_e - \mathbf{S} \right] \mathrm{d}\Omega_e = \oint_{\Gamma_e} \mathbf{\Phi}_e^T \left[\mathbf{A}_n \mathbf{q}_e - \mathbf{f}^\star(\mathbf{q}_e, \mathbf{q}_e^{\mathrm{ext}}) \right] \mathrm{d}\Gamma_e \,, \tag{4}$$

where $\mathbf{q}_e$ corresponds to the approximated solution vector over each element. The numerical flux $\mathbf{f}^\star$, the normal flux matrix $\mathbf{A}_n = \mathbf{A}_x n_x + \mathbf{A}_y n_y$, and the outward-pointing normal $\mathbf{n} = (n_x, n_y)$ are defined along the element interface Γ_e. It can be seen that all the terms are expressed in terms of the local solution $\mathbf{q}_e$, except for the numerical flux used to evaluate the contour integral, which involves the solution vector of the neighboring element $\mathbf{q}_e^{\mathrm{ext}}$ from the other side of the interface. Indeed, since the test functions are discontinuous across the element boundaries, the acoustic fields on each point of the interface Γ_e are multiply defined; the purpose of the numerical flux is to couple the elements and to ensure continuity of the fields.

An upwind numerical flux is used in this work, with optimal dispersion properties, which can be constructed by considering the propagation direction of the characteristic waves of the problem. Due to the hyperbolicity of the propagation equations (3), an eigendecomposition of the normal flux matrix can be performed as $\mathbf{A}_n = \mathbf{W}\mathbf{\Lambda}\mathbf{W}^{-1}$, with

$$\mathbf{W} = \begin{bmatrix} 0 & 1 & 1 \\ n_y & n_x/\rho_0 c & -n_x/\rho_0 c \\ -n_x & n_y/\rho_0 c & -n_y/\rho_0 c \end{bmatrix} \quad \text{and} \quad \mathbf{\Lambda} = \begin{bmatrix} u_n & 0 & 0 \\ 0 & u_n + c & 0 \\ 0 & 0 & u_n - c \end{bmatrix},$$

with u_n the projection of the local wind vector along the normal $\mathbf{n}$. This eigendecomposition allows a definition of the characteristic waves $\tilde{\mathbf{q}} = \mathbf{W}^{-1}\mathbf{q}$ as

$$\tilde{\mathbf{q}} = \begin{Bmatrix} \tilde{q}_u \\ \tilde{q}_a^+ \\ \tilde{q}_a^- \end{Bmatrix} = \begin{Bmatrix} n_y v_x - n_x v_y \\ \left(p + \rho_0 c\, \mathbf{v} \cdot \mathbf{n}\right)/2 \\ \left(p - \rho_0 c\, \mathbf{v} \cdot \mathbf{n}\right)/2 \end{Bmatrix}, \tag{5}$$

where $\tilde{q}_a^+$ and $\tilde{q}_a^-$ correspond to the strength of the acoustic waves leaving and entering the element, respectively, and $\tilde{q}_u$ to the strength of the vorticity wave associated with the wind (e.g., [12]). The convection speed and direction of the characteristic waves along the normal $\mathbf{n}$ is given by the corresponding diagonal entries of $\mathbf{\Lambda}$: the acoustic waves propagate in opposite directions (assuming a subsonic flow) at the speed $|u_n \pm c|$, while the vorticity wave is convected by the normal component of the wind.

The upwind flux can thus be constructed on physical grounds, since the waves leaving the elements should only depend on the local solution $\mathbf{q}_e$, while the waves entering the elements should only depend on the external solution $\mathbf{q}_e^{\mathrm{ext}}$. Mathematically, this amounts to defining the numerical flux along the interface as

$$\mathbf{f}^\star(\mathbf{q}_e, \mathbf{q}_e^{\mathrm{ext}}) = \mathbf{W}\left[\mathbf{\Lambda}^+ \mathbf{W}^{-1} \mathbf{q}_e + \mathbf{\Lambda}^- \mathbf{W}^{-1} \mathbf{q}_e^{\mathrm{ext}} \right], \tag{6}$$

where $\mathbf{\Lambda}^+$ and $\mathbf{\Lambda}^-$ contains the positive and negative eigenvalues, respectively. It can also be shown that Eq. (6) can be rewritten, using the relation $\mathbf{\Lambda}^\pm = (\mathbf{\Lambda} \pm |\mathbf{\Lambda}|)/2$, as [8]

$$\mathbf{f}^\star(\mathbf{q}_e, \mathbf{q}_e^{\mathrm{ext}}) = \frac{1}{2}\left[\mathbf{A}_n \mathbf{q}_e + \mathbf{A}_n \mathbf{q}_e^{\mathrm{ext}} + \mathbf{W}|\mathbf{\Lambda}|\mathbf{W}^{-1}(\mathbf{q}_e - \mathbf{q}_e^{\mathrm{ext}}) \right], \tag{7}$$

where $|\mathbf{\Lambda}|$ is a diagonal matrix containing the absolute value of the elements of $\mathbf{\Lambda}$. This expression is more convenient in practice since the sign of the eigenvalues may depend on the wind direction. After some algebra,

[1] For consistency with the PSTD solution in the hybrid solver, the conservative form of the LEE is implicitly considered; this amounts to a few additional physical assumptions that are reasonable in the context of atmospheric sound propagation (see, e.g., [2]).

the exact upwind flux associated with the propagation equations (3), for each acoustic variable, reads

$$
\begin{aligned}
f_p^\star &= c\left([[p]] + \rho_0 c < \mathbf{v} > \cdot \mathbf{n}\right) + u_n\left(< p > + \rho_0 c\,[[\mathbf{v}]] \cdot \mathbf{n}\right) , \\
f_{v_x}^\star &= n_x\, c\left(\frac{< p >}{\rho_0 c} + [[\mathbf{v}]] \cdot \mathbf{n}\right) + u_n\left(\frac{[[p]]}{\rho_0 c} + < v_x >\right) + |u_n|\left([[v_x]] - n_x\,[[\mathbf{v}]] \cdot \mathbf{n}\right) , \\
f_{v_y}^\star &= n_y\, c\left(\frac{< p >}{\rho_0 c} + [[\mathbf{v}]] \cdot \mathbf{n}\right) + u_n\left(\frac{[[p]]}{\rho_0 c} + < v_y >\right) + |u_n|\left([[v_y]] - n_x\,[[\mathbf{v}]] \cdot \mathbf{n}\right) .
\end{aligned}
\tag{8}
$$

The following operators were defined to simplify the expressions:

$$
< \mathbf{q}_e >= \frac{\mathbf{q}_e + \mathbf{q}_e^{\text{ext}}}{2} \qquad \text{and} \qquad [[\mathbf{q}_e]] = \frac{\mathbf{q}_e - \mathbf{q}_e^{\text{ext}}}{2} , \tag{9}
$$

which correspond to the mean value and to the difference between the solution on both sides of the interface, respectively. In the absence of wind ($u_n = 0$), the numerical flux presented in other studies can be recovered [13].

2.3. Boundary conditions

The numerical flux is used to couple adjacent elements. However, boundary conditions need to be considered if the element interface lies on an acoustic boundary. Similarly to the derivation of the upwind flux, the boundary conditions can be implemented based on the propagation direction of the characteristic waves: at any given time, the waves associated with a positive eigenvalue (leaving the element) do not carry any information about the boundary, while the waves associated with a negative eigenvalue need to be specified [14].

For the acoustic characteristic waves, the reflected wave $\tilde{q}_a^-$ can be computed as a function of the incident wave $\tilde{q}_a^+$, based on the impulse response function of the plane-wave reflection coefficient $r(t)$ defining the (locally-reacting) boundary material. This requires the computation of a convolution integral for each boundary point of the form

$$
\tilde{q}_a^-(t) = \int_{-\infty}^{t} \tilde{q}_a^+(\tau)\, r(t-\tau) \mathrm{d}\tau \, . \tag{10}
$$

This general formulation is also known as a time-domain impedance boundary condition and can allow frequency-dependent material properties [15, 16]. Equation (10) is sufficient in the context of outdoor sound propagation since the (mean) wind is assumed to fulfill the no-slip condition on the acoustic boundaries. The vorticity wave $\tilde{q}_u$ also needs to be specified whenever the local wind vector is directed inwards ($u_n < 0$), in which case the condition $\tilde{q}_u = 0$ is arbitrarily used. This condition is not physically relevant in this work, but is still required mathematically and numerically to promote stability.

The boundary conditions can then be enforced weakly by computing the virtual external solution $\mathbf{q}_e^{\text{ext}}$ to be used in the definition of the numerical flux [Eq. (7)], based on the updated characteristic waves, as $\mathbf{q}_e^{\text{ext}} = \mathbf{W}\,\tilde{\mathbf{q}}$.

2.4. Perfectly Matched Layers

Absorbing conditions are required at the edges of the computational domain to simulate open boundaries. The Perfectly Matched Layers (PML) methodology is used in this work, as first presented by Bérenger for electromagnetics [17].

Numerous PML implementations can be found in the literature, based on either split or unsplit acoustic variables. However, it was found in this work that split-variable approaches are hardly compatible with the present DG formulation, since the upwind numerical flux given in Eq. (8) cannot be easily split into different components, due to the presence of wind. A convolutional PML approach (C-PML) formulated in unsplit variables [18, 19] was thus adapted and successfully implemented into the current DG framework. The treatment proposed by Hu [20], in aeroacoustics, to stabilize the PML formulation in the presence of a mean flow was also found to be compatible with the convolutional approach, and is thus considered in this work.

2.5. Implementation

As presented in details in [6], an approximate solution to the strong formulation of the LEE given in Eq. (4) can now be obtained numerically by considering the *nodal* expansion of the solution $\mathbf{q}_e$, as

$$\mathbf{q}_e(\mathbf{r}, t) \approx \sum_{n=1}^{N_p} \psi_n(\mathbf{r})\, \mathbf{q}_e(\mathbf{r}_n, t)\,, \tag{11}$$

with N_p interpolating polynomials $\mathbf{\Psi}_e = \{\psi_1, \psi_2, \ldots, \psi_{N_p}\}$. By defining the test functions $\mathbf{\Phi}_e$ in the variational formulation to be equal to the basis functions $\mathbf{\Psi}_e$, a semi-discrete formulation can be obtained in terms of the nodal values of the solution vector $\mathbf{q}_e(\mathbf{r}_n, t)$. In this work, the spatial integration is then performed with a quadrature-free approach [21], using quadrilateral elements. The solution at each interpolation nodes is then advanced in time with an optimized 8-stage explicit Runge-Kutta method [22].

3 Hybrid PSTD-DG solver

The DG formulation presented in the previous section is able to accurately describe the propagation of sounds in complex outdoor conditions, including the effects of the atmosphere, the ground, and potential buildings. Still, the application of the DG method in this context can be challenging in terms of computational resources, since acoustic waves can travel over thousands of wavelengths. As shown in a previous study [9], the DG method can be hybridized with the cost-effective Fourier PSTD method to lessen this limitation.

3.1. The Fourier pseudospectral time-domain method

The Fourier PSTD method consists in computing spatial derivatives in the wavenumber domain [1]. More specifically, the physical domain is discretized on a Cartesian grid so that each derivative can be estimated with the use of a one-dimensional discrete spatial Fourier transform; the inverse transform is then applied to go back to the time domain. The solution is then advanced in time with a time integration scheme. The Fourier PSTD method is generally very computationally efficient since the spatial Fourier transforms can be computed with the Fast Fourier Algorithm (FFT).

In this work, this procedure is directly applied to the LEE [Eq. (3)]; the incorporation of wind in PSTD is straightforward, so the reader is referred to [9] for more details about the method. The time integration is performed with an optimized 6-stage explicit Runge-Kutta method [23]. The same convolutional PML formulation as for the DG solver is implemented to truncate the computational domain.

3.2. Hybrid methodology

The application of discrete Fourier transforms in PSTD imply a spatial periodicity of the solution, which renders the implementation of complex boundaries difficult. In the hybrid solver, the PSTD method is thus used in the bulk of the domain, which should take up most of the computational domain for long-range outdoor configurations, while the DG method is used close to the boundaries.

The hybridization procedure is not presented in detail since it is similar to the no-wind case; a thorough description can be found in [9]. It consists in spatially coupling the PSTD and DG solvers in a region where both domains overlap. This coupling zone allows for exchanging the solution values between the two solvers, as illustrated on Figure 1. The mesh in the DG coupling zone is structured and conformal with the PSTD grid to simplify the exchange of data. In this work, the implementation of a mild anti-aliasing modal filter [6] in the DG domain was also found necessary for long-term stability of the hybrid model.

4 Verification

This section aims at assessing the accuracy of the hybrid model in the presence of wind.

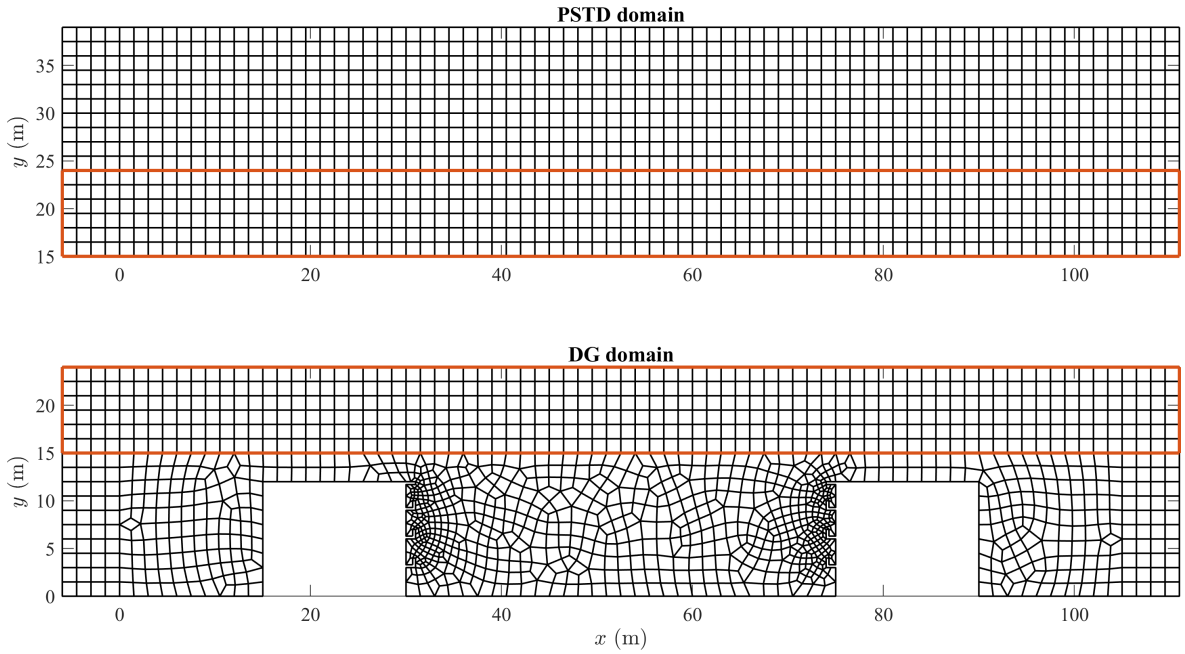

Figure 1: Schematic example of PSTD (top) and DG (bottom) meshes in the hybrid solver for an urban configuration featuring buildings with balconies. The coupling zone (generally with a thickness of 20 to 30 points), where data is exchanged between the PSTD and DG domains, is indicated in red. In DG, the mesh is also structured near the left and right outer boundaries to simplify the PML formulation.

4.1. Free-field propagation with a uniform subsonic flow

The first test case consists in the propagation of an acoustic pulse in free field, in the presence of a constant horizontal flow towards the direction of increasing x, defined as $\mathbf{u} = (0.5c, 0)$. This flow is not directly relevant to outdoor sound propagation but allows assessing the hybrid solver for extreme wind conditions, since the LEE are able provide an accurate description of the problem and since a simple analytical solution can be obtained.

The simulation is performed with the hybrid PSTD-DG model inside a computational domain of size 160 m by 170 m, with an unstructured quadrilateral mesh of characteristic length equal to about 1 m for DG; this amounts to about 15 points per wavelengths at a frequency of 100 Hz. The DG solver is fourth-order accurate in space, and both solvers are fourth-order accurate in time. The bottom and top halves of the domain are solved with DG and PSTD, respectively, with the coupling zone in-between. The domain is surrounded by PML to truncate the domain. The acoustic pulse is generated from a Gaussian initial pressure distribution located inside the DG domain, at $(x, y) = (-30, 30)$ m, and two receivers are located at $(30, 30)$ m and $(30, 100)$ m, inside the DG and PSTD domains, respectively. The pulse propagates during 600 time iterations.

Figure 2 shows snapshots of the simulated pressure field every 50 time iterations; the pulse expands and is convected streamwise, and is eventually absorbed by the PML layers without any noticeable reflections. The signal recorded by both microphones is shown on Figure 3. The frequency content varies between the microphones because of the Doppler effect due to the convection of the initial disturbance. A perfect agreement is found with the analytical solution, both in the time and the frequency domains, across the entire frequency range of interest.

This indicates that the model is able to account for wind convection, and that the coupling procedure does not introduce significant errors for this simple test case. Additional tests were also carried out with the source inside the PSTD domain; a perfect agreement was found in all cases. It should be noted that the current implementation of the hybrid solver does not allow for a strong vertical wind component inside the PML layers in the coupling zone, which could result in instabilities; no loss of accuracy was observed with wind otherwise.

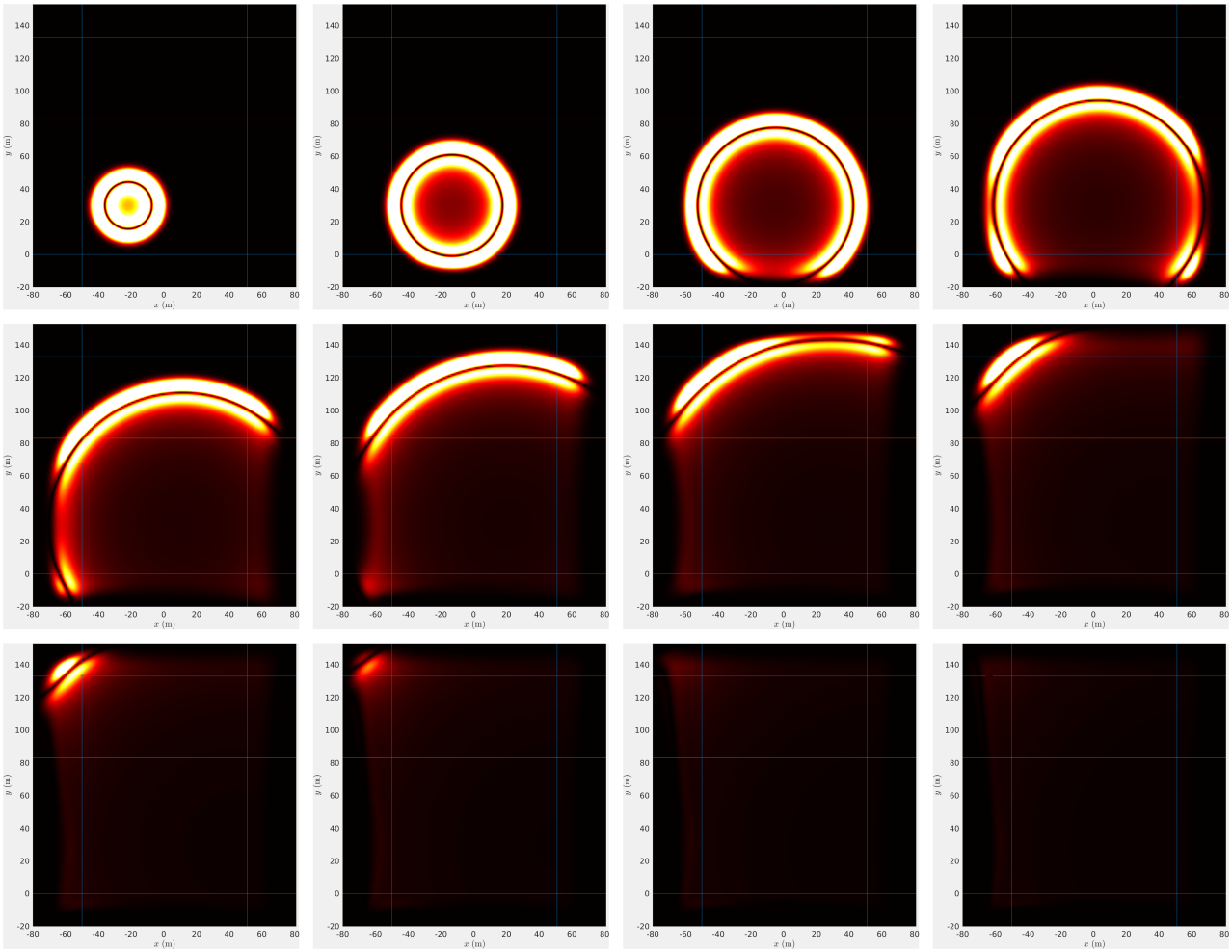

Figure 2: Simulated pressure field with a uniform horizontal flow, every 50 time iterations. The amplitude is normalized by $\sqrt{ct}$. The horizontal red line delimits the upper boundary of the (DG) coupling zone; the thin blue lines indicate the PML interface with air.

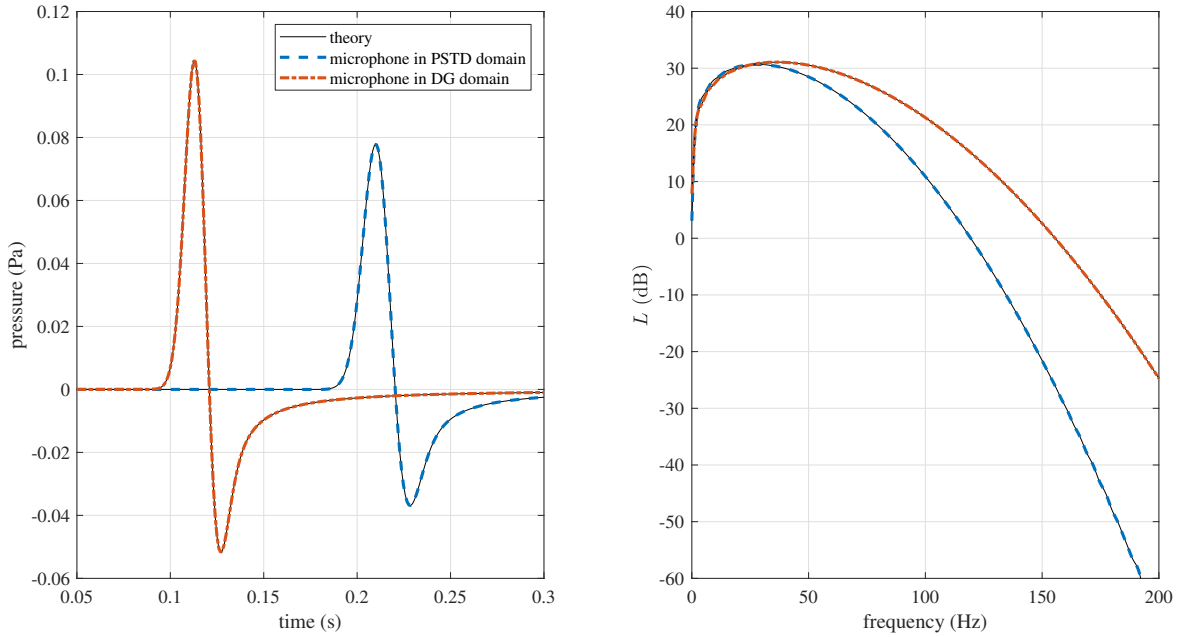

Figure 3: Recorded signals in the PSTD and DG domains in the time (left) and frequency (right) domains. The analytical solution is based on [2] and [24].

4.2. Long-range propagation in a stratified atmosphere

This more complex test case features long-range sound propagation over a flat absorbing grass ground with downward refraction. A vertical profile of horizontal wind is considered, based on the Monin-Obukhov similarity theory, with a frictional velocity of $0.5\,\mathrm{m\,s^{-1}}$ and a roughness length of 5 mm; this amounts to a wind strength of approximately $7.5\,\mathrm{m\,s^{-1}}$ at a height of 2 m. The ground impedance is modeled with the variable porosity model [25], with an effective air flow resistivity of $25\,\mathrm{kPa\,s\,m^{-2}}$ and a porosity decay rate of $50\,\mathrm{m^{-1}}$; these parameters were obtained from in situ ground impedance measurements in a grass field in previous studies [26, 27]. Unlike the previous test case, no simple and accurate analytical solution exists. A solver based on a carefully validated finite-difference time-domain (FDTD) model [27] is thus used here for comparison with the hybrid PSTD-DG solver.

The source is located at a height of 2 m, and three microphones are placed downwind, 100 m horizontally from the source, at a height of 2, 10 and 20 m, respectively. The DG mesh has a characteristic length of 10 cm; the PSTD-DG simulation is expected to be accurate up to about 2 kHz. The FDTD parameters are chosen to provide numerical errors of a similar order of magnitude.

Figure 4 displays the PSTD-DG pressure field at different times. The signals recorded by the three microphones are shown on Fig. 5. A very good agreement with FDTD is found in the time domain. In the frequeny domain (not shown, for brevity), the level differences are smaller than 0.5 dB within the investigated frequency range. Similar discrepancies are found without wind, which indicates than the wind does not introduce significant numerical errors. The FDTD results without wind are also displayed, for comparison.

5 Conclusion

The hybrid PSTD-DG model presented in [9] was successfully extended to take into account a moving inhomogeneous atmosphere by explicitly solving the LEE in the presence of wind, as opposed to the effective sound speed approximation; the latter would imply angular constraints which could limit the applicability of the model in the context of outdoor sound propagation [10]. A full revision of the DG formulation was required. The new hybrid solver was validated for a free field configuration with a strong uniform wind, and for a long-range configuration with downward refraction due to a vertical wind gradient above an absorbing ground. A

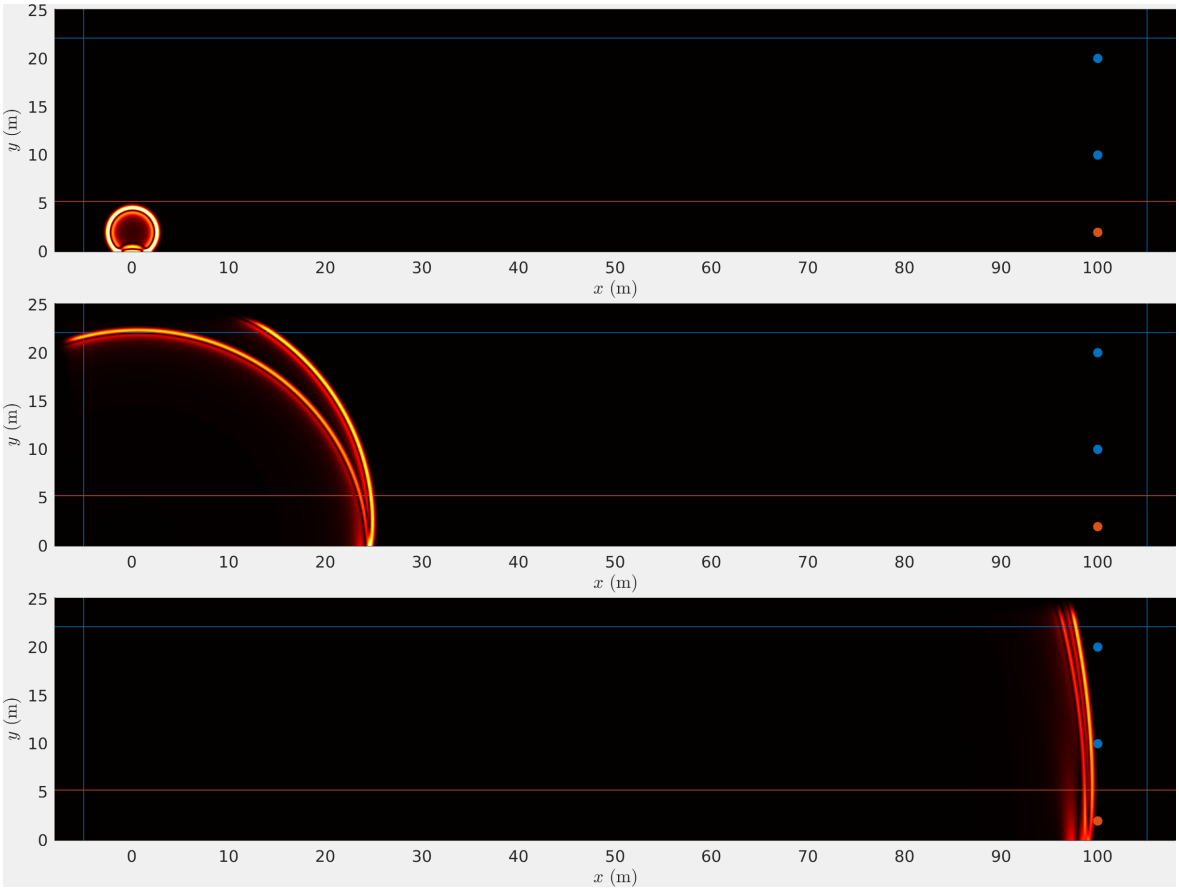

Figure 4: Simulated pressure field for a downwind propagation over an absorbing (grass) ground (normalized amplitude). The blue and red dots indicate the location of the microphones.

perfect agreement was found in the time and frequency domains, suggesting that the incorporation of wind is not a source of error. Additional validation data are however needed in order to assess the model in urban configurations.

Acknowledgements

The authors would like to thank Raúl Pagán Muñoz and Sai Trikootam for their contribution to this work.

References

[1] M. Hornikx, R. Waxler, and J. Forssén. The extended Fourier pseudospectral time-domain method for atmospheric sound propagation. *The Journal of the Acoustical Society of America*, 128(4):1632–1646, Oct 2010.

[2] D. Dragna, B. Cotté, P. Blanc-Benon, and F. Poisson. Time-domain simulations of outdoor sound propagation with suitable impedance boundary conditions. *AIAA Journal*, 49(7):1420–1428, Jul 2011.

[3] L. Ehrhardt, S. Cheinet, D. Juvé, and P. Blanc-Benon. Evaluating a linearized Euler equations model for strong turbulence effects on sound propagation. *The Journal of the Acoustical Society of America*, 133(4):1922–1933, 2013.

[4] T. Van Renterghem. Efficient outdoor sound propagation modeling with the finite-difference time-domain (FDTD) method: a review. *International Journal of Aeroacoustics*, 13(5-6):385–404, Oct 2014.

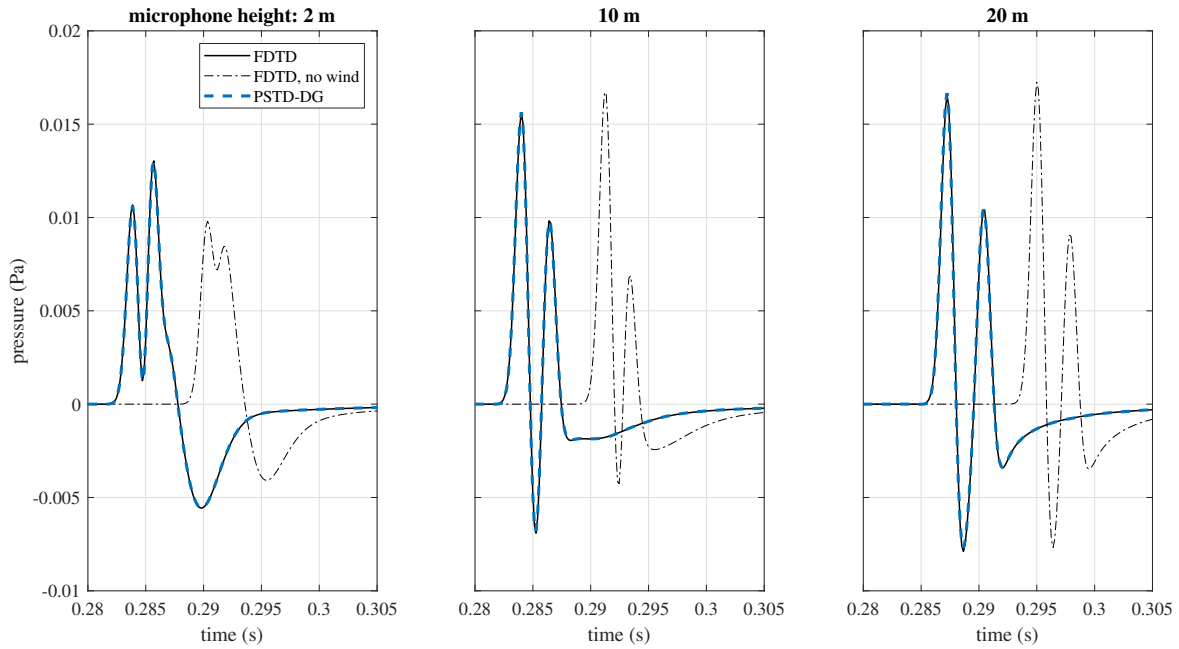

Figure 5: Pressure waveforms recorded by the three microphones with the hybrid solver and with an FDTD solver, with and without wind.

[5] M. Hornikx. Ten questions concerning computational urban acoustics. *Building and Environment*, 106:409–421, Sep 2016.

[6] T. Warburton J. S. Hesthaven. *Nodal Discontinuous Galerkin Methods*. Springer-Verlag GmbH, 2007.

[7] S. Minisini, E. Zhebel, A. Kononov, and W. A. Mulder. Local time stepping with the discontinuous Galerkin method for wave propagation in 3D heterogeneous media. *GEOPHYSICS*, 78(3):T67–T77, May 2013.

[8] M. Williamschen. *Time-domain DGM for turbofan exhaust noise predictions*. PhD thesis, University of Southampton, Aug 2018.

[9] R. Pagán Muñoz and M. Hornikx. Hybrid Fourier pseudospectral/discontinuous Galerkin time-domain method for wave propagation. *Journal of Computational Physics*, 348:416–432, Nov 2017.

[10] E. M. Salomons. *Computational atmospheric acoustics*. Springer Science + Business Media, 2001.

[11] V. E. Ostashev, D. K. Wilson, L. Liu, D. F. Aldridge, N. P. Symons, and D. Marlin. Equations for finite-difference, time-domain simulation of sound propagation in moving inhomogeneous media and numerical implementation. *The Journal of the Acoustical Society of America*, 117(2):503–517, 2005.

[12] G. Gabard and E. J. Brambley. A full discrete dispersion analysis of time-domain simulations of acoustic liners with flow. *Journal of Computational Physics*, 273:310–326, Sep 2014.

[13] H. Wang, I. Sihar, R. Pagán Muñoz, and M. Hornikx. Room acoustics modelling in the time-domain with the nodal discontinuous Galerkin method. *The Journal of the Acoustical Society of America*, 145(4):2650–2663, Apr 2019.

[14] R. L. Higdon. Initial-boundary value problems for linear hyperbolic system. *SIAM Review*, 28(2):177–217, Jun 1986.

[15] D. Dragna, P. Pineau, and P. Blanc-Benon. A generalized recursive convolution method for time-domain propagation in porous media. *The Journal of the Acoustical Society of America*, 138(2):1030–1042, Aug 2015.

[16] H. Wang and M. Hornikx. Time-domain impedance boundary condition modeling with the discontinuous

Galerkin method for room acoustics simulations. *The Journal of the Acoustical Society of America*, 147(4):2534–2546, Apr 2020.

[17] J.-P. Bérenger. A perfectly matched layer for the absorption of electromagnetic waves. *Journal of Computational Physics*, 114(2):185–200, Oct 1994.

[18] D. Komatitsch and R. Martin. An unsplit convolutional perfectly matched layer improved at grazing incidence for the seismic wave equation. *GEOPHYSICS*, 72(5):155–167, Sep 2007.

[19] A. Modave, J. Lambrechts, and C. Geuzaine. Perfectly matched layers for convex truncated domains with discontinuous Galerkin time domain simulations. *Computers & Mathematics with Applications*, 73(4):684–700, Feb 2017.

[20] F. Q. Hu. A Perfectly Matched Layer absorbing boundary condition for linearized Euler equations with a non-uniform mean flow. *Journal of Computational Physics*, 208(2):469–492, Sep 2005.

[21] H. L. Atkins and C.-W. Shu. Quadrature-free implementation of discontinuous Galerkin method for hyperbolic equations. *AIAA Journal*, 36(5):775–782, May 1998.

[22] T. Toulorge and W. Desmet. Optimal Runge–Kutta schemes for discontinuous Galerkin space discretizations applied to wave propagation problems. *Journal of Computational Physics*, 231(4):2067–2091, Feb 2012.

[23] C. Bogey and C. Bailly. A family of low dispersive and low dissipative explicit schemes for flow and noise computations. *Journal of Computational Physics*, 194(1):194–214, Feb 2004.

[24] C. Bogey and C. Bailly. Three-dimensional non-reflective boundary conditions for acoustic simulations: far field formulation and validation test cases. *Acta Acustica united with Acustica*, 88(4):463–471, 2002.

[25] K. Attenborough, I. Bashir, and S. Taherzadeh. Outdoor ground impedance models. *The Journal of the Acoustical Society of America*, 129(5):2806–2819, May 2011.

[26] S. Cheinet, M. Cosnefroy, F. Königstein, W. Rickert, M. Christoph, S. L. Collier, A. Dagallier, L. Ehrhardt, V. E. Ostashev, A. Stefanovic, T. Wessling, and D. K. Wilson. An experimental study of the atmospheric-driven variability of impulse sounds. *The Journal of the Acoustical Society of America*, 144(2):822–840, aug 2018.

[27] M. Cosnefroy. *Propagation of impulsive sounds in the atmosphere: numerical simulations and comparison with experiments*. PhD thesis, École Centrale de Lyon, 2019 (in French).